PNAS RESEARCH ARTICLE | BIOPHYSICS AND COMPUTATIONAL BIOLOGY

Activation mechanism of the μ-opioid receptor by an allosteric modulator

Shun Kaneko[a,b], Shunsuke Imai[a], Nobuaki Asao[a,b], Yutaka Kofuku[b], Takumi Ueda[b], and Ichio Shimada[a,1]

Edited by Peter Wright, Department of Integrative Structural and Computational Biology, Scripps Research Institute, La Jolla, CA; received December 3, 2021; accepted March 4, 2022

Allosteric modulators of G-protein-coupled receptors (GPCRs) enhance signaling by binding to GPCRs concurrently with their orthosteric ligands, offering a novel approach to overcome the efficacy limitations of conventional orthosteric ligands. However, the structural mechanism by which allosteric modulators mediate GPCR signaling remains largely unknown. Here, to elucidate the mechanism of μ-opioid receptor (MOR) activation by allosteric modulators, we conducted solution NMR analyses of MOR by monitoring the signals from methionine methyl groups. We found that the intracellular side of MOR exists in an equilibrium between three conformations with different activities. Interestingly, the populations in the equilibrium determine the apparent signaling activity of MOR. Our analyses also revealed that the equilibrium is not fully shifted to the conformation with the highest activity even in the full agonist-bound state, where the intracellular half of TM6 is outward-shifted. Surprisingly, an allosteric modulator for MOR, BMS-986122, shifted the equilibrium toward the conformation with the highest activity, leading to the increased activity of MOR in the full agonist-bound state. We also determined that BMS-986122 binds to a cleft in the transmembrane region around T162 on TM3. Together, these results suggest that BMS-986122 binding to TM3 increases the activity of MOR by rearranging the direct interactions of TM3 and TM6, thus stabilizing TM6 in the outward-shifted position which is favorable for G-protein binding. These findings shed light on the rational developments of novel allosteric modulators that activate GPCRs further than orthosteric ligands alone and pave the way for next-generation GPCR-targeting therapeutics.

GPCR | solution NMR | allosteric modulator

Significance

The allosteric modulators, which bind to nonorthosteric sites to enhance the signaling activities of G-protein-coupled receptors (GPCRs), are new candidates for GPCR-targeting drugs. Our solution NMR analyses of the μ-opioid receptor (MOR) revealed that the MOR activity was determined by a conformational equilibrium between three conformations. Interestingly, an allosteric modulator shifted the equilibrium toward a conformation with the highest activity to a level that cannot be reached by orthosteric ligands alone, leading to the increased activity of MOR. Our NMR analyses also identified the binding site of the allosteric modulator, including the residues contributing to the regulation of the equilibrium. These findings provide insights into the rational developments of novel allosteric modulators.

G-protein-coupled receptors (GPCRs) are seven-transmembrane receptors that play critical roles in a broad range of cellular responses by coupling with various effectors, such as heterotrimeric G proteins or arrestins (1). More than 30% of clinically used therapeutics target GPCRs by binding to the orthosteric sites of the receptors (2), where their intrinsic ligands bind, highlighting the pharmacological and biological importance of GPCRs. GPCR ligands have different efficacy levels, which correlate with their therapeutic properties (3). The orthosteric ligands that exhibit the highest efficacies among the known ligands are classified as the full agonists. Despite extensive screening efforts, orthosteric ligands that harbor higher efficacies than those of the currently known full agonists have been rarely identified (4, 5). This fact clearly illustrates the limitation of the GPCR activity that the orthosteric ligands can elicit. On the other hand, in many GPCRs a residue substitution increases the activity of the GPCR in the full agonist-bound state (6–8). These previous observations indicated that the activities of GPCRs bound to their full agonists are not the highest levels attainable by GPCRs. Accordingly, allosteric modulators, which enhance the affinity of orthosteric ligands and/or the signaling activity of GPCRs in complex with orthosteric ligands by binding to nonorthosteric sites, have attracted pharmaceutical interest as a novel approach to enhance the activation of GPCRs beyond the capability of the orthosteric agonists alone (9). Several allosteric modulators of GPCRs as well as some three-dimensional structures of GPCRs in complex with allosteric modulators have been reported (10–15). However, these static structures in crystals or ice do not exhibit significant differences as compared to those in the absence of the allosteric modulators. Therefore, the structural mechanism of GPCR activation of allosteric modulators remains still largely unknown, hampering rational developments of allosteric modulator-based GPCR-targeting therapeutics.

The μ-opioid receptor (MOR) is one of the class A GPCRs stimulated by opioid peptides, which are released in response to pain or stress states to induce analgesia (16, 17). Opioid analgesics, such as morphine, are orthosteric agonists of MOR that stimulate it to induce analgesia. Some allosteric modulators of MOR have been reported

Author affiliations: [a]Center for Biosystems Dynamics Research, RIKEN, Kanagawa 230-0045, Japan; and [b]Graduate School of Pharmaceutical Sciences, The University of Tokyo, Tokyo 113-0033, Japan

Author contributions: S.K., S.I., Y.K., T.U., and I.S. designed research; S.K., S.I., and N.A. performed research; S.K., S.I., T.U., and I.S. analyzed data; and S.K., S.I., and I.S. wrote the paper.

The authors declare no competing interest.

This article is a PNAS Direct Submission.

[1]To whom correspondence may be addressed. Email: ichio.shimada@riken.jp.

This article contains supporting information online at http://www.pnas.org/lookup/suppl/doi:10.1073/pnas.2121918119/-/DCSupplemental.

Published April 11, 2022.

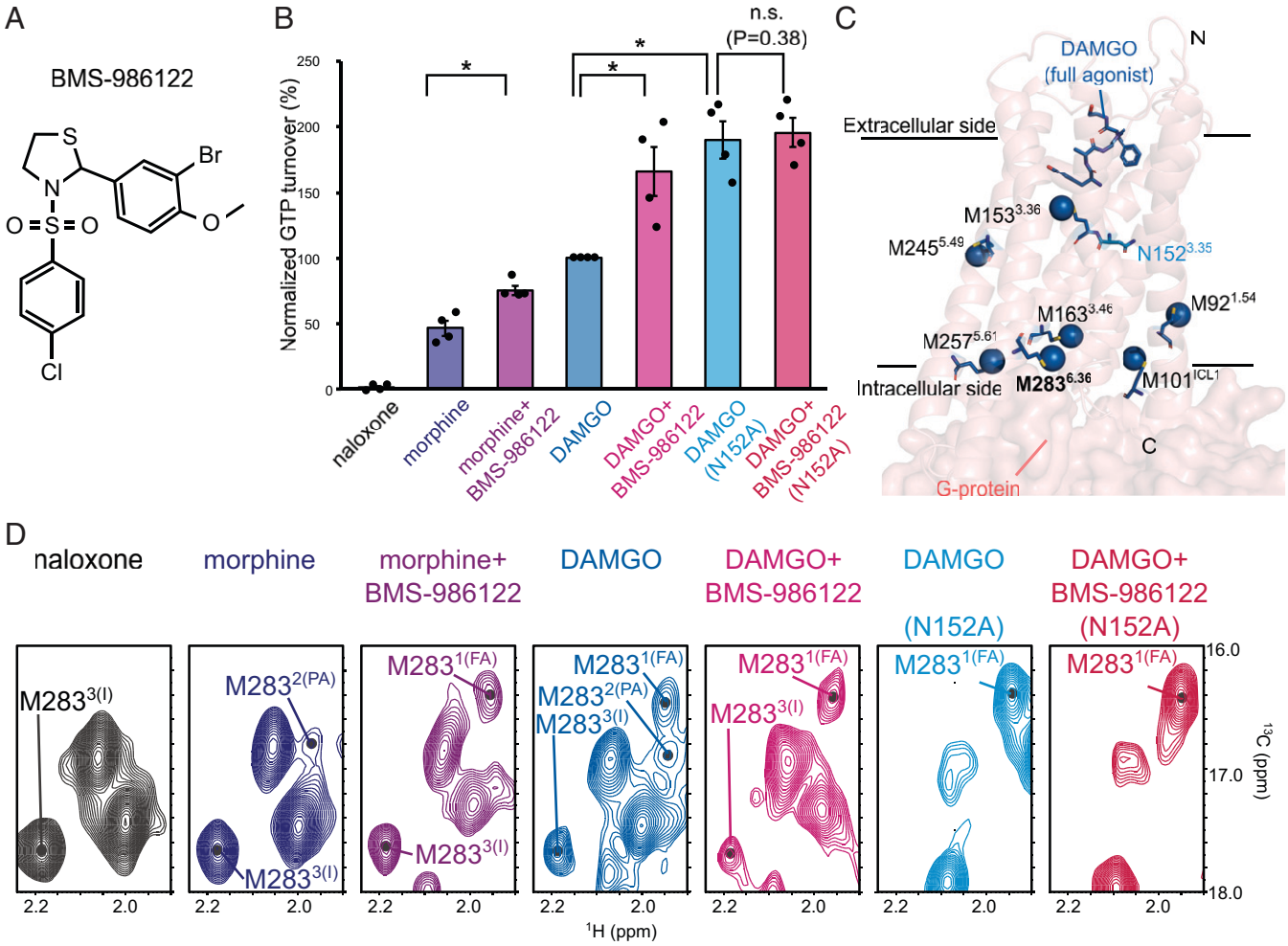

Fig. 1. The signaling activities and ^{1}H-^{13}C HMQC spectra of MOR. (*A*) The chemical structure of BMS-986122. (*B*) The signaling activities of MOR/Δ6M or MOR/Δ6M/N152A, in the antagonist naloxone-bound, the partial agonist morphine-bound, and the full agonist DAMGO-bound states, in the absence and presence of the allosteric modulator BMS-986122, measured by a GTP turnover assay. Data are presented as the percentage of stimulation of the full agonist DAMGO-bound state of MOR/Δ6M. Data shown are means ± SEM of four independent experiments, each performed in duplicate. Comparisons of data were performed by using an unpaired two-tailed Welch's *t* test with significance denoted by asterisks: *$P < 0.05$; no significance (n.s.): $P \geq 0.05$. (*C*) The distribution of methionine residues of MOR/Δ6M in the structure of MOR bound to the full agonist DAMGO and G protein (PDB ID code 6DDF). (*D*) ^{1}H-^{13}C HMQC signals of M283 of MOR/Δ6M or MOR/Δ6M/N152A under each condition. The peak tops of the resonances from M283 are indicated with dots.

(18–21), and a compound termed BMS-986122 (Fig. 1*A*) exhibited the best subtype-selective allosteric modulator activity (18, 22). BMS-986122 elicited analgesic effects in mice by boosting the endogenous opioid peptide pathway (23), supporting the proposal that allosteric modulators of MOR could be a novel type of analgesic (24). Three-dimensional structures of MOR in the absence of allosteric modulators have been reported (25–27) and revealed that the G_i protein binds to a cavity on the cytoplasmic side formed by the rotation and outward shift of the intracellular half of transmembrane helix (TM) 6, as also observed for GPCR structures bound to G proteins (28–30). Based on these structural analyses, as proposed for other GPCRs, we suggest that the intracellular half of TM6 in MOR shifts outward upon activation. However, the binding site of the allosteric modulator for MOR and the mechanism by which it increases the activity of MOR remain unknown.

Here, to clarify the structural basis for MOR activation by the model allosteric modulator BMS-986122, we used NMR spectroscopy, which allows observation of biomolecules in solution (6, 31–37), to analyze the dynamic structures and functions of MOR. Previously, Wüthrich's group observed NMR signals from site-specifically modified ^{19}F-probes and revealed the conformational equilibrium in the β_2-adrenergic receptor underlying the biased signaling pathway (38). Kobilka's group used ε-^{13}C methionine labeling with NMR observations to show the conformational heterogeneity of the β_2-adrenergic receptor bound to various orthosteric ligands (39). Grzesiek's group used NMR with backbone ^{15}N-valine labeling and characterized the allosteric activation pathway between the ligand binding pocket and the intracellular side of the thermostabilized β_1-adrenergic receptor (40). Hagn's group observed the NMR signals from chemically modified ^{13}C-MMTS probes introduced in a neurotensin receptor variant and identified its function-related equilibria (41). In this study, by using NMR spectroscopy, we identified a previously unknown equilibrium at the intracellular half of TM6, between three conformations with different activities. Interestingly, the NMR data revealed that the equilibrium in the full agonist DAMGO-bound state is not completely shifted to the conformation with the highest activity, where the intracellular half of TM6 is outward-shifted. These findings indicated that MOR in the DAMGO-bound state is not activated to the level it could potentially reach. Our analyses also revealed that BMS-986122 increased the population of this conformation in the equilibrium, thus enhancing the activity of MOR. BMS-986122 binds to a cavity in the transmembrane region of MOR, where T162 on TM3 plays a

critical role in the activation by BMS-986122 as well as the subtype selectivity. These data also suggested that BMS-986122 rearranges the interactions between TM3 and TM6, which determine the apparent activity of MOR to perturb the equilibrium, resulting in the increased activity. Importantly, this mechanism of MOR hyperactivation by BMS-986122 explains the mechanism underlying the increased activity by point mutations introduced on TM3 or TM6, reported for other GPCRs. Together, these results provide an approach for the rational development of allosteric modulators of GPCRs that cannot be sufficiently activated by conventional orthosteric ligands.

Results

Characterization of the Allosteric Modulation by BMS-986122. In this study, we used our previous reported human MOR construct, MOR/Δ6M (*SI Appendix*, Fig. S1; see *SI Appendix*, *SI Methods* for details) (6). First, the effects of the allosteric modulator BMS-986122 on MOR/Δ6M embedded in lauryl maltose neopentyl glycol (LMNG) micelles were investigated (*SI Appendix*, Fig. S2). The MOR/Δ6M binding affinity of the full agonist DAMGO, which has efficacy comparable to the intrinsic opioid peptide (18), increased by 1.9-fold in LMNG micelles in the presence of BMS-986122 (*SI Appendix*, Fig. S2*B*). This result indicated that the mutations introduced in the MOR/Δ6M construct do not affect the reactivity for BMS-986122. We then quantitatively investigated the positive allosteric modulating activity of BMS-986122 on the stimulation of the guanosine triphosphate (GTP) turnover rate of the heterotrimeric G_i protein, using MOR/Δ6M bound to various ligands (Fig. 1*B* and *SI Appendix*, Figs. S2 *C–E* and S3). When normalized by the GTP turnover rate of the G_i protein in the presence of MOR/Δ6M in the full agonist DAMGO-bound state, the activity of MOR/Δ6M in the antagonist naloxone-bound state was 0%, confirming that MOR/Δ6M exhibits the efficacy-dependent G_i-protein-stimulating activity. Furthermore, the MOR/Δ6M activity increased from 46 to 74% in the partial agonist morphine-bound state, and from 100 to 166% in the full agonist DAMGO-bound state, by the addition of a saturating amount (10 μM) of BMS-986122. These values are in good agreement with those of the MOR construct without six methionine mutations introduced in MOR/Δ6M, where the DAMGO-binding affinity increased by 3.9-fold, and the G_i-protein-stimulating activities increased from 55 to 88% in the partial agonist morphine-bound state and 91 to 133% in the full agonist DAMGO-bound state upon the addition of BMS-986122 (*SI Appendix*, Fig. S2). These results corroborated that the six methionine mutations do not alter how BMS-986122 modulates the G-protein-signaling activity of MOR. Intriguingly, the activity of the N152A variant of MOR/Δ6M, which has higher activity than the parental MOR/Δ6M (6), did not increase by the addition of BMS-986122 in the full agonist DAMGO-bound state (190% and 196% in the absence and presence of BMS-986122, respectively) (Fig. 1*B* and *SI Appendix*, Fig. S2*F*). These quantitative analyses indicated that the MOR/Δ6M activity increases by the addition of BMS-986122 even in the full agonist DAMGO-bound state, and the degrees of enhancement by BMS-986122 differ depending on the orthosteric ligands bound to MOR.

NMR Resonances of MOR/Δ6M Methionine Residues. MOR/Δ6M harbors a total of seven methionine residues, $M92^{1.54}$, $M101^{ICL2}$, $M153^{3.36}$, $M163^{3.46}$, $M245^{5.49}$, $M257^{5.61}$, and $M283^{6.36}$ [Fig. 1*C*; superscripts refer to Ballesteros–Weinstein numbering (42)]. Among them, M283 resides at the intracellular tip of TM6, suggesting that the NMR signals of M283 may reflect the conformational changes of TM6, which directly interacts with the G_i protein. To observe the NMR resonances of the methionine residues in MOR/Δ6M with high sensitivity and resolution, we labeled it with [αβγ-^{2}H, methyl-^{13}C]methionine in a highly deuterated background in the insect cell expression system that we previously established (6, 43). We obtained ^{1}H-^{13}C heteronuclear multiple quantum coherence (HMQC) spectra of the isotope-labeled MOR/Δ6M and MOR/Δ6M/N152A, under the same set of ligands and the allosteric modulator BMS-986122 conditions as the GTP turnover assay (*SI Appendix*, Fig. S4 *A–D*). The assignments of the signals from M283 were established by comparing the spectra with those of the variants, in which M283 was substituted with a leucine residue (*SI Appendix*, Fig. S5). M283 exhibited three signals in the full agonist DAMGO-bound state, at the ^{1}H and ^{13}C chemical shifts of 1.96 and 16.4 ppm, 1.96 and 16.8 ppm, and 2.20 and 17.6 ppm (Fig. 1*D*). Hereafter, we refer to these signals as M283 (1), M283 (2), and M283 (3), in the order of their ^{13}C chemical shifts. The relative intensities of these signals changed upon decreasing the temperature from 298 K to 288 K (*SI Appendix*, Fig. S6), indicating that they undergo a chemical exchange process between three local conformations on a time scale slower than the chemical shift differences of these states. A comparison of the spectra in the absence and presence of BMS-986122 under three conditions, MOR/Δ6M in the partial agonist morphine-bound state, MOR/Δ6M in the full agonist DAMGO-bound state, and MOR/Δ6M/N152A in the DAMGO-bound state, revealed that the intensities of the M283 (1), M283 (2), and M283 (3) signals varied depending on the conditions. These results indicated that the populations in the equilibrium were altered among these conditions. Indeed, under any conditions tested the NMR signals from M283 were observed at one or more of the three positions, indicating that the conformational equilibrium exists under all these conditions. Interestingly, the addition of BMS-986122 altered the populations for MOR/Δ6M but not for MOR/Δ6M/N152A in the full agonist DAMGO-bound state.

Next, we compared the intensities of M283 (1), M283 (2), and M283 (3) (Fig. 1*D*) with the signaling activity of MOR (Fig. 1*B*). In the antagonist naloxone-bound state, only the M283 (3) signal was observed. This demonstrated that the M283 (3) signal reflects a conformation lacking the G-protein-stimulating activity, since MOR did not exhibit signaling activity. Therefore, we hereafter refer to the M283 (3) signal as $M283^{I}$ (for the Inactivated conformation). In the full agonist DAMGO-bound state of MOR/Δ6M/N152A in the presence of BMS-986122, where the highest signaling activity was observed, only the M283 (1) signal was observed. Under the conditions where intermediate signaling activities were observed, i.e., in the partial agonist morphine- and the full agonist DAMGO-bound states, the intensity of the M283 (1) signal decreased, and the M283 (2) signal was observed. Upon the addition of BMS-986122 or the introduction of the N152A mutation, which both increase the MOR activity, the intensities of M283 (1) and M283 (2) increased and decreased, respectively. These observations indicated that the M283 (1) and M283 (2) signals reflect the conformations with the highest and intermediate activities, respectively. Therefore, we hereafter refer to the M283 (1) signal as $M283^{FA}$ (for the Fully Activated conformation) and the M283 (2) signal as $M283^{PA}$ (for the Partially Activated conformation). By optimizing the relative activity of each conformation to clarify the apparent activity under these

conditions, relative activities of 0.00, 0.64, and 1.00 for the inactivated, partially activated, and fully activated conformations were obtained, respectively, with an R^2 value of 0.96 (*SI Appendix*, Fig. S7). Together, these results demonstrated that the three signals from M283 reflect distinct conformations with different activities, and the equilibrium between these conformations determines the apparent activity of MOR.

For M257 on TM5, which is the closest methionine residue to M283 (Fig. 1*C*), changes in signal line widths depending on the conditions were observed (*SI Appendix*, Fig. S8). The line widths of M257 in the full agonist DAMGO-bound state sharpened as the temperature was decreased from 298 K to 288 K, which is the same change observed upon the addition of BMS-986122 at 298 K (*SI Appendix*, Fig. S6). Because the correspondence of the spectral changes upon decreasing the temperature and adding BMS-986122 was consistent with that observed for M283, these results indicate that both of these neighboring residues, M257 and M283, are involved in the same conformational equilibrium on the intracellular side of MOR (Fig. 1*C* and *SI Appendix*, Fig. S6). The other signals from the methionine residues did not exhibit changes that suggested population shifts in the conformational equilibrium (*SI Appendix*, Fig. S9). However, it should be noted that the perturbations of the signals of M153, M163, and M245 upon the addition of BMS-986122 suggested that the local environments of these residues, which are near the BMS-986122 binding site, were affected by the interaction with BMS-986122 by itself (*SI Appendix*, Fig. S9; see below).

Characterization of Conformations in the Function-Related Equilibrium by Solvent Paramagnetic Relaxation Enhancement Analyses. To examine the structural characteristics of each conformation with different activity in the equilibrium of MOR, the solvent accessibilities of the methionine residues were examined by solvent paramagnetic relaxation enhancement (PRE) experiments (44, 45). In these experiments, Gd-diethylenetriamine pentaacetic acid-bismethylamide (Gd-DTPA-BMA), a freely diffusable paramagnetic probe (44), was added to the sample containing MOR. The PRE effects arising from the magnetic dipolar interactions between the nuclear spin and the unpaired electron spin of the diffusing paramagnetic probe enhance the relaxation of the nuclear spins. This leads to the intensity reduction of the NMR signals of the solvent-exposed residues in a manner dependent on the averaged distance from the paramagnetic probes in solution. First, we conducted the solvent PRE analyses for MOR in the antagonist β-funaltrexamine (β-FNA)–bound state (*SI Appendix*, Fig. S10 *A*–*C*), for which a crystal structure has been reported (25). We compared the solvent PRE effects observed for methyl groups of methionine residues with the solvent accessibilities in the crystal structure (*SI Appendix*, Fig. S10 *D* and *E*), which were calculated based on the Hwang–Freed model to predict solvent PRE effects, as reported previously (44, 45). This solvent accessibility value decreases as the methyl group becomes more exposed to the solvent, for which the larger PRE effects from the paramagnetic probe Gd-DTPA-BMA are predicted. In this experiment, we used the MOR construct that lacks the Δ6M mutations, in order to increase the number of signals analyzed. The signals of the detergent LMNG methyl groups in micelles, which serve as the internal reference of the shielded methyl groups, exhibited an intensity reduction ratio of 0.33 ± 0.01 (*SI Appendix*, Fig. S10*C*). The solvent accessibility of each methionine residue MOR in the antagonist β-FNA–bound state revealed by our solvent PRE analyses correlated with that of each methionine residue calculated from the crystal structure of MOR bound to β-FNA (25) (*SI Appendix*, Fig. S10*E*, R^2 = 0.97; see *SI Appendix*, *SI Methods* for details).

We then used solvent PRE analyses to examine the solvent accessibilities of M283 in each conformation of the function-related equilibrium. We estimated that the exchange rates between the three conformations are slower than the chemical shift differences of the $M283^{I}$, $M283^{PA}$, and $M283^{FA}$ signals, i.e., slower than 20 s^{-1}. The differences in the transverse PRE effects arising from the paramagnetic probe Gd-DTPA-BMA in the solvent can reportedly be larger than these exchange rates (44), i.e., as large as 50 s^{-1}, indicating that the slow chemical exchange process does not average the solvent PRE effects experienced in each conformation. Therefore, the PRE effects for $M283^{I}$, $M283^{PA}$, and $M283^{FA}$ should reflect the solvent accessibilities of the methyl group of M283 in the inactivated, partially activated, and fully activated conformations, respectively. The ^{1}H-^{13}C HMQC spectra of MOR/Δ6M bound to the full agonist DAMGO were then acquired in the absence and presence of the paramagnetic probe Gd-DTPA-BMA (Fig. 2 *A* and *B* and *SI Appendix*, Fig. S4*E*). The intensity reduction ratio of the detergent LMNG methyl group shielded in micelles was 0.36 ± 0.01 (Fig. 2*C*) and was similar to that in the antagonist β-FNA–bound state (*SI Appendix*, Fig. S10*C*; 0.33 ± 0.01). The signal intensity reduction ratios of the three signals from M283 before and after the addition of Gd-DTPA-BMA were 0.62 ± 0.17, 0.11 ± 0.25, and 0.33 ± 0.12 for $M283^{FA}$, $M283^{PA}$, and $M283^{I}$, respectively (Fig. 2*C*). Of these, only $M283^{FA}$ exhibited an intensity reduction ratio higher than that of the detergent LMNG methyl, indicating that the methyl group of M283 is only exposed to the solvent in the fully activated conformation. Using the correlation plot obtained for the β-FNA–bound state (*SI Appendix*, Fig. S10*E*), the solvent accessibilities estimated from the intensity reduction ratios of $M283^{FA}$ were calculated to be 2.2 Å. A comparison of this value with the solvent accessibilities of $Met^{6.36}$ in the MOR or δ opioid receptor structures deposited in the Protein Data Bank (PDB) (25–27, 46–48) revealed that a solvent accessibility of 2.2 Å can only be possible in the structures with the outward-shifted intracellular half of TM6 (Fig. 2*D* and *SI Appendix*, Fig. S11). These results strongly suggest that the intracellular half of TM6 is shifted outward in the fully activated conformation, whereas it is shifted inward in the inactivated and partially activated conformations, as compared to the fully activated conformation.

Identification of the BMS-986122 Binding Site. To examine the mechanism by which the allosteric modulator BMS-986122 alters the populations in the structural equilibrium at TM6, we sought to identify the BMS-986122 binding site by identifying the methionine residues with NMR chemical shifts perturbed upon the addition of BMS-986122 (Fig. 3*A* and *SI Appendix*, Figs. S9 and S12). As mentioned above, we observed significant chemical shift perturbations or extreme line broadening for the M153, M163, and M245 signals upon the addition of 100 μM of BMS-986122 to 10 to 20 μM of MOR/Δ6M, which results in the bound population of 98%, considering the fact that the binding constant of BMS-986122 for MOR/Δ6M is 1.7 μM (Fig. 3 *B* and *C* and *SI Appendix*, Figs. S3 and S9). The line broadening of the NMR signals upon the addition of BMS-986122 is caused by the local dynamics of MOR/Δ6M in the BMS-986122–bound state. The perturbations of these NMR signals indicated that the local environments of these residues, which are in the vicinity of the BMS-986122 binding site, are

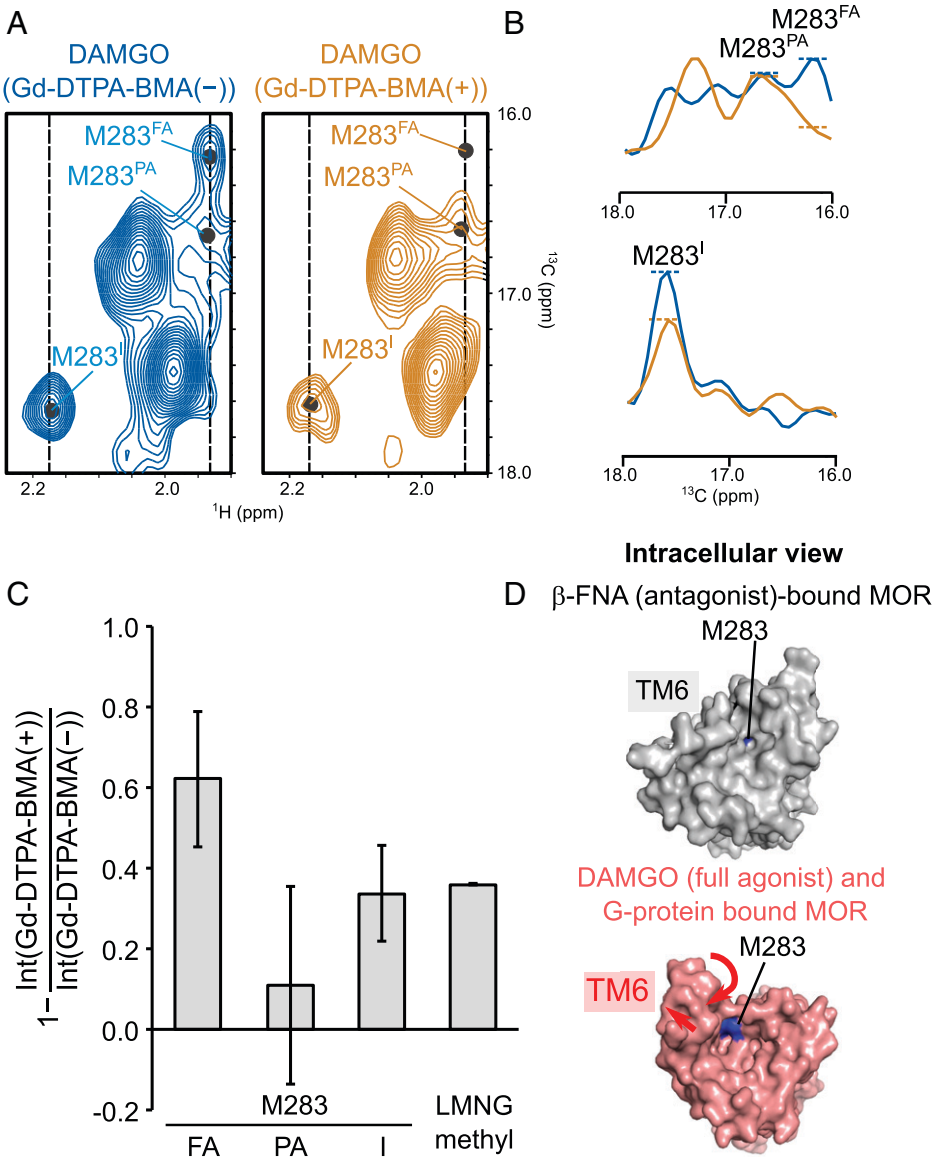

Fig. 2. The solvent PRE analyses of MOR in the full agonist DAMGO-bound state. (*A*) ^{1}H-^{13}C HMQC signals of M283 of MOR/Δ6M in the full agonist DAMGO-bound state in the absence of the paramagnetic probe Gd-DTPA-BMA (blue) and in the presence of 2 mM Gd-DTPA-BMA (orange). The NMR spectra were acquired with an Avance-900 spectrometer (900 MHz ^{1}H). The peak tops of the resonances from M283 in the absence of Gd-DTPA-BMA are indicated with dots. (*B*) Cross-sections of the ^{1}H-^{13}C signals at the dashed lines indicated in *A*. (*C*) Plots of the intensity reduction ratios calculated from the signal intensities of M283, in the presence and absence of Gd-DTPA-BMA. The bars represent the experimental errors, calculated from the root sum squares of the ratios of the noise level to the signal intensity. (*D*) Intracellular views of the surface representation of MOR structures in complex with the antagonist β-FNA (gray, PDB ID code 4DKL) or the full agonist DAMGO and the G protein (pink, PDB ID code 6DDF). The surface of M283 is indicated in blue. The M283 residue in MOR bound to DAMGO and the G protein is exposed to the solvent by the outward shift of the intracellular side of TM6, as compared with the structure of MOR bound to the antagonist.

affected by the interaction with BMS-986122. To identify BMS-986122 binding site, methionine residues were introduced by point mutations near these residues, at the positions of W158, L196, L234, and I240 (*SI Appendix*, Figs. S1*A* and S12). One new signal was observed in the spectra of the MOR/Δ6M/W158M, MOR/L196M, MOR/L234M, and MOR/Δ6M/I240M variants in the full agonist DAMGO-bound state (*SI Appendix*, Fig. S12 *A* and *B*), indicating that the signal was from the introduced methionine. Among these four variants, upon the addition of BMS-986122 only the signal from M158 of the W158M variant exhibited a chemical shift difference as large as 0.17 ppm (*SI Appendix*, Fig. S12*C*). These results suggest that W158 resides close to the binding interface, while L196, L234, and I240 do not. When mapped on the structure of MOR in complex with the full agonist DAMGO and the G_i protein (27), M153, W158, M163, and M245 all exist near a cleft on the molecular surface in the transmembrane region, and T162 resides at the bottom of the cleft (Fig. 3*C* and *SI Appendix*, Fig. S12*D*). Intriguingly, T162 is a unique residue in MOR and not conserved in the other opioid receptor subtypes, δ opioid receptor and κ opioid receptor, which both have methionine residue in the corresponding positions (*SI Appendix*, Fig. S13). Considering that BMS-986122 exhibits subtype selectivity for MOR (18, 22), we substituted T162 with methionine and analyzed the changes in the NMR spectra of this variant, MOR/Δ6M/T162M, in the full agonist DAMGO-bound state, in the presence and absence of BMS-986122. As a result, the M153 and M245 signals did not disappear, and the M162 and M163 signals did not exhibit chemical shift changes, indicating that T162M mutation abolished the interaction of MOR with

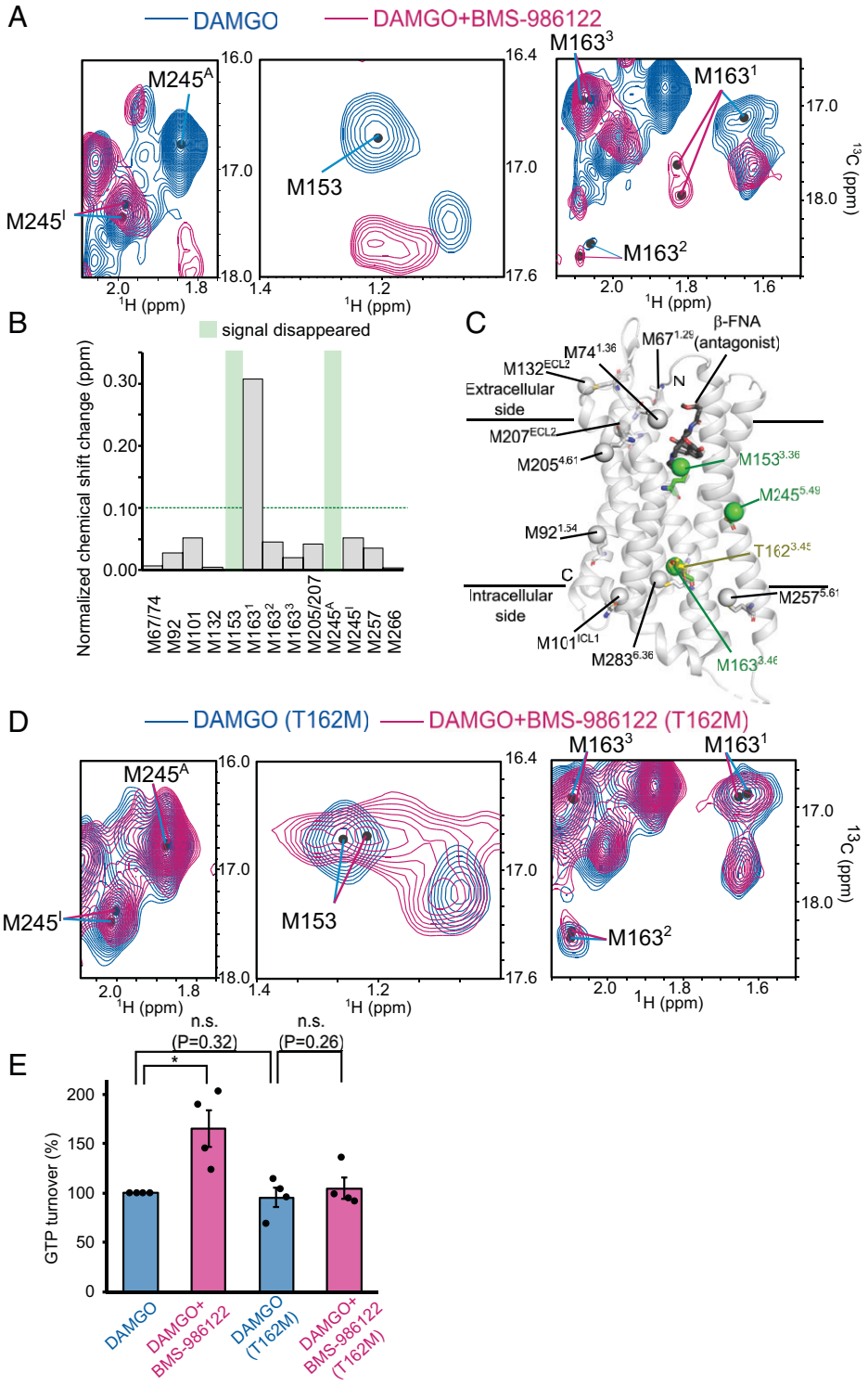

Fig. 3. Elucidation of the BMS-986122 binding site on MOR. (*A*) ^{1}H-^{13}C HMQC signals of M245, M153, and M163 of MOR/Δ6M in the full agonist DAMGO-bound state in the absence (blue) and presence (magenta) of the allosteric modulator BMS-986122. The peak tops of the resonances from M245, M153, and M163 are indicated with dots. The resonances of M245^{A} and M153 were not observed in the DAMGO-bound state in the presence of BMS-986122. (*B*) Chemical shift differences of the methionine ^{1}H-^{13}C HMQC signals, except for M283, which showed the population shift in the equilibrium, between the presence and absence of BMS-986122 in the full agonist DAMGO-bound state. The chemical shift differences in the ^{1}H and ^{13}C directions were normalized with the equation (32) $\sqrt{\delta_{1H}^2 + (\delta_{13C}^2/3.5)^2}$, where the normalization factor 3.5 is the ratio of the SD of the methionine of ^{1}H and ^{13}C methyl chemical shifts deposited in the Biological Magnetic Resonance Data Bank (https://bmrb.io/). For the split signals in M163 (1), the major signals were used to calculate the chemical shift differences. Residues highlighted with green backgrounds are those not observed in the full agonist DAMGO-bound state in the presence of BMS-986122. (*C*) Mapping of the perturbed residues on the crystal structure of MOR bound to an antagonist (PDB ID code 4DKL). Green spheres represent carbon atoms of methyl groups of the methionine residues that exhibited chemical shift differences larger than 0.1 ppm or extreme line broadening upon the addition of BMS-986122. (*D*) ^{1}H-^{13}C HMQC signals of M245, M153, and M163 of MOR/Δ6M/T162M in the full agonist DAMGO-bound state in the absence (blue) and presence (magenta) of BMS-986122. The peak tops of the resonances from M245, M153, and M163 are indicated with dots. (*E*) The signaling activities of MOR/Δ6M or MOR/Δ6M/T162M in the full agonist DAMGO-bound state in the absence and presence of BMS-986122, measured by a GTP turnover assay. Data are presented as the percentage of stimulation of the DAMGO-bound state of MOR/Δ6M. Data shown are means ± SEM of four independent experiments, each performed in duplicate. Comparisons of data were performed by using an unpaired two-tailed Welch's *t* test with significances denoted by asterisks: *$P < 0.05$; no significance (n.s.): $P \geq 0.05$.

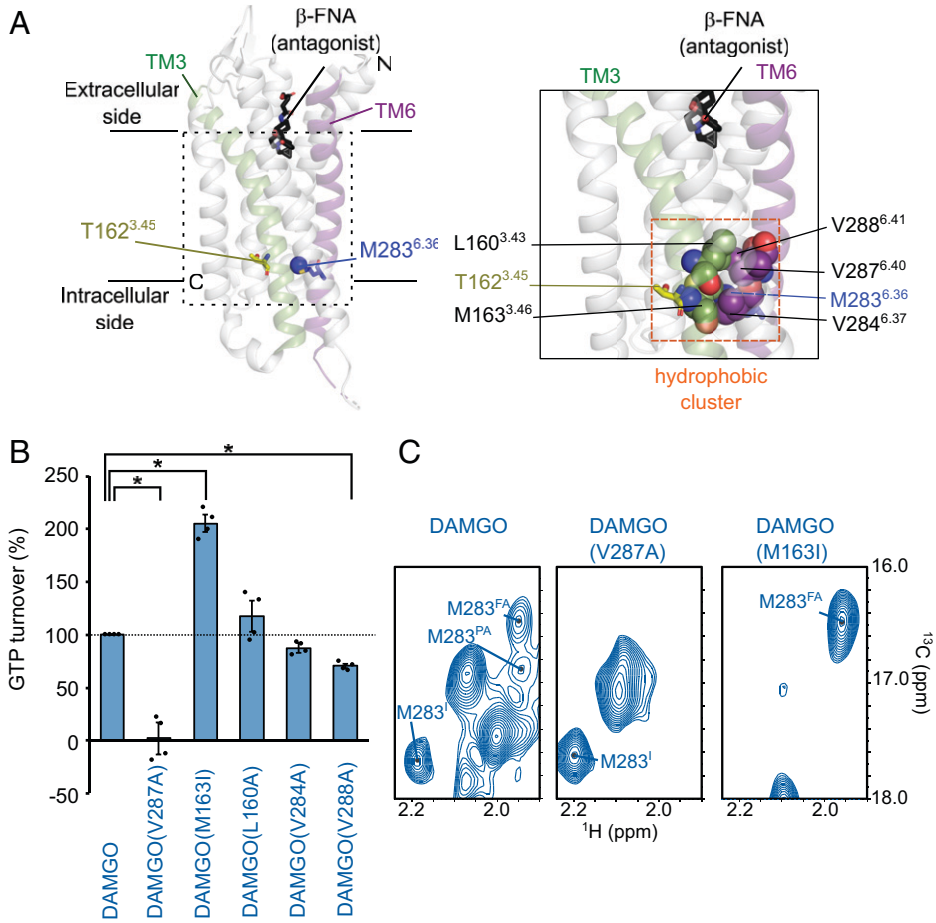

Fig. 4. Effects of mutations introduced in the interface between TM3 and TM6 on the signaling activity and the conformational equilibrium of MOR. (*A*, *Left*) Mapping of T162, which composes the binding site of the allosteric modulator BMS-986122, and M283, for which the conformational equilibrium was observed, on the structure of MOR bound to the antagonist β-FNA (PDB ID code 4DKL). (*A*, *Right*) Mapping of the hydrophobic residues composing the interface of TM3 and TM6, namely, L160, M163, V284, V287, and V288. (*B*) The signaling activities of MOR/Δ6M/M245V or its variants in the full agonist DAMGO-bound state measured by a GTP turnover assay. M245V was introduced to alleviate the NMR signal overlaps. Data are presented as the percentage of stimulation of the DAMGO-bound state of MOR/Δ6M/M245V. Data shown are means ± SEM of four independent experiments, each performed in duplicate. Comparisons of data were performed by using an unpaired two-tailed Welch's *t* test, with significance denoted by asterisks: **P* < 0.05; no significance (n.s.): *P* ≥ 0.05. (*C*) ^{1}H-^{13}C HMQC signals of M283 of MOR/Δ6M, MOR/Δ6M/M245V/V287A, or MOR/Δ6M/M245V/M163I under each condition. The centers of the resonances from M283 are indicated with dots. In the V287A variant, the resonances of M283^{FA} and M283^{PA} were not observed. In the M163I variant, the resonances of M283^{PA} and M283^{I} were not observed.

BMS-986122 (Fig. 3*D* and *SI Appendix*, Fig. S3*F*). Furthermore, the addition of BMS-986122 to the MOR/Δ6M/T162M variant did not enhance the G_i-stimulating activity (Fig. 3*E*). These results indicate that BMS-986122 recognizes the surface of MOR where the residue on TM3, T162, is exposed to the lipid membrane side, and that the subtype selectivity of BMS-986122 for MOR stems from the recognition of T162, which is unique to MOR among the opioid receptors.

Mechanism of the Conformational Equilibrium Shift by BMS-986122. To further explore the mechanism by which BMS-986122 binding to the region containing T162 in TM3 modulates the conformational equilibrium in TM6, we investigated the effects of mutations on the interface between TM3 and TM6. Considering that TM3 directly contacts TM6 through a conserved hydrophobic cluster composed of L160, M163, V284, V287, and V288 in the crystal structure of the antagonist β-FNA–bound state (Fig. 4*A*), we introduced point mutations to the abovementioned five residues, L160A, M163I, V284A, V287A, and V288A, to rearrange the hydrophobic cluster and investigated the signaling activities of these variants in the full agonist DAMGO-bound state (Fig. 4*B*). The introduction of the M163I and V287A variants results in higher (205%) and lower (2%) signaling activities, respectively (Fig. 4*B*). In the NMR spectra, only the M283^{FA} signal was observed from M283 for the M163I variant, whereas only the M283^{I} signal was observed for the V287A variant (Fig. 4*C* and *SI Appendix*, Fig. S4*G*). The signaling activities of the M163I and V287A variants were 196% and 0%, respectively, as calculated from the populations of the NMR signals of M283 using the weighting factor determined from the optimization (*SI Appendix*, Fig. S7), in good agreement with the activities determined from the GTP turnover assay (205% and 2%, respectively) (Fig. 4*B*). These data demonstrated that mutations of M163 on TM3 or V287 on TM6 alter the activity by modulating the populations of the function-related equilibrium. The substitution of M163 with an isoleucine increases the volume of the side chain, whereas the alanine substitution of V287 decreases it. These changes correlate with the increase and decrease of the population of the fully activated conformation, where the intracellular half of TM6 is outwardly shifted. Therefore, the mutations shift the conformational equilibrium by increasing or decreasing the steric clashes within the hydrophobic cluster that directly pushes TM6 outward. Since BMS-986122 binds to the region containing T162, which is next to M163 in the hydrophobic cluster, and induces an effect on the

conformational equilibrium and activity similar to the M163I mutation, BMS-986122 binding might shift the conformational equilibrium by increasing the steric clash on the hydrophobic cluster, as the M163I mutation increases the size of the side chain.

Discussion

Our NMR experiments revealed that MOR exists in a conformational equilibrium between the three conformations with different activities, namely, fully activated, partially activated, and inactivated conformations, and that the populations of these conformations define the apparent signaling activity of MOR. This function-related equilibrium was observed for the signals from M257 and M283 on the intracellular side of MOR, at which MOR directly interacts with the G protein (Fig. 1*C*). Various orthosteric ligands and the model allosteric modulator, BMS-986122, change the signaling activity of MOR by shifting this equilibrium (Fig. 1 *B* and *D*). It should be noted here that the signal from M245 on TM5 (Fig. 1*C*), where a conformational equilibrium regulating signaling balances between the G protein and arrestin pathways was observed in our previous report (6), exhibited the extreme line broadening upon the addition of BMS-986122 because the local environment of M245 residue was affected by the direct interaction with BMS-986122 (Fig. 3*A*). Our analyses of the solvent PRE effects demonstrated that the inactivated conformation corresponds to the crystal structure of MOR in complex with the antagonist β-FNA (*SI Appendix*, Fig. S10), while the intracellular half of TM6 is outward-shifted in the fully activated conformation and inward-shifted in the partially activated and inactivated conformations (Fig. 2). In the crystal structure of MOR in complex with β-FNA (25), two aromatic residues, Y338$^{7.53}$ and F345$^{8.50}$, are located close to the methyl group of M283, and the arrangement of the aromatic residues revealed that the ^{1}H chemical shift of M283^{I} is downfield-shifted due to the ring-current shift effects (49) (*SI Appendix*, Fig. S14). The ^{1}H chemical upfield shift of M283^{PA}, as compared to M283^{I}, indicated that the methyl group of M283 is farther from the two aromatic residues in the partially activated conformation, although TM6 is inward-shifted as in the inactivated conformation (Fig. 2). Accordingly, the most probable conformational change that moves the methyl group of M283 farther from the two aromatic residues would be the rotation of the intracellular half of TM6, because such rotations at the hinge formed by a conserved proline residue, P297$^{6.50}$, have been observed for GPCRs bound to agonists (25–27, 35, 45) (*SI Appendix*, Fig. S14). Taken together, the intracellular half of TM6 is closed and not rotated in the inactivated, closed and rotated in the partially activated, and open and rotated in the fully activated conformations (Fig. 5*A*). Since G proteins bind to the cavity formed by the outward shift of the intracellular half of TM6 (27), the finding that the intracellular half of TM6 is outward-shifted accounts for the structural basis of the higher signaling activity of the fully-activated conformation, as also suggested for other GPCRs (28–30).

Our NMR study revealed that the allosteric modulator BMS-986122 enhances the MOR activity by increasing the population of the fully activated conformation in the conformational equilibrium to a level that cannot be reached by orthosteric ligands (Fig. 1 *B* and *D*). On the other hand, the chemical shifts of the M283 signal in each conformation did not change upon the addition of BMS-986122, suggesting that BMS-986122 binding does not change the conformation of MOR by itself. Therefore, the reason why the static structures of other GPCRs in complex with their allosteric modulators do not exhibit significant structural differences, as compared to those in the absence of the allosteric modulators, may be because these structures were obtained under conditions where the dynamic properties of GPCRs were largely suppressed by crystallization, complexing with intracellular binders, or thermostabilizing mutations, to stabilize them in one of the possible snapshot structures in the conformational equilibrium.

Our NMR study also showed that the activity of MOR in the full agonist DAMGO-bound state does not reach its potential maximum because the inactivated and partially activated conformations are considerably populated in this state (Fig. 1*D*), in agreements with previous reports for several GPCRs studied by solution NMR spectroscopy (38–41). This was strongly supported by the observation that the activity of the N152A variant, which assumes only the fully activated conformation in the DAMGO-bound state, was higher than that of MOR/Δ6M and was not further enhanced by the addition of BMS-986122 (Fig. 1). These findings clearly demonstrate that the orthosteric ligand alone is not capable of shifting the conformational equilibrium of the MOR/Δ6M completely to the fully activated conformation. The reason why even the full agonists, with the highest efficacies among the known orthosteric ligands, cannot elicit the highest activity of MOR is probably because the interactions of the orthosteric ligands with the extracellular half of TM6 cannot be efficiently converted to the outward shifting of the intracellular half of TM6, due to the disconnection of the two halves at the hinge formed by the conserved proline residue, P297 (Fig. 5). BMS-986122 binding to the cleft around T162 on TM3 and the substitution of N152 on TM3 to Ala both increase the population of the fully activated conformation, where the intracellular half of TM6 is outward-shifted. These results indicate that two different perturbations on TM3 result in the same conformational equilibrium shift at TM6. Furthermore, two mutations introduced into the interface between TM3 and TM6 also altered the population of the equilibrium: The M163I variant showed an equilibrium shift toward the fully activated conformation and higher activity, whereas the V287A variant showed a shift toward the inactivated conformation and lower activity (Fig. 4 *B* and *C*). Based on these results, we propose that the hydrophobic cluster between TM3 and TM6 defines the equilibrium and thus the apparent activity of MOR (Fig. 5*B*).

Interestingly, in some GPCRs that harbor the conserved hydrophobic cluster formed by the residues on TM3 and TM6, substituting these residues reportedly increase the activity in the full agonist-bound state. For instance, substituting the valine in CXCR1 corresponding to V287 of MOR with an asparagine and the threonine in CB1 corresponding to M163 of MOR with an isoleucine increases the signaling activities beyond that of the wild type in the full agonist-bound state (7, 8). The detailed mechanism of these increases in the activity by the point mutations, which has been quite elusive, can be explained by the population shifts in the function-related conformational equilibrium, as in the case of the addition of BMS-986122 to MOR in the full agonist DAMGO-bound state. Therefore, in these cases, the interactions of compounds with the transmembrane surface on TM3 would enable the hyperactivation of GPCRs in the orthosteric full agonist-bound state, in a manner similar to the mutations. Thus, the mechanism of allosteric modulator action revealed in the present study would be a general remedy to enable the activation of GPCRs beyond the capability of the orthosteric full agonist alone. These results

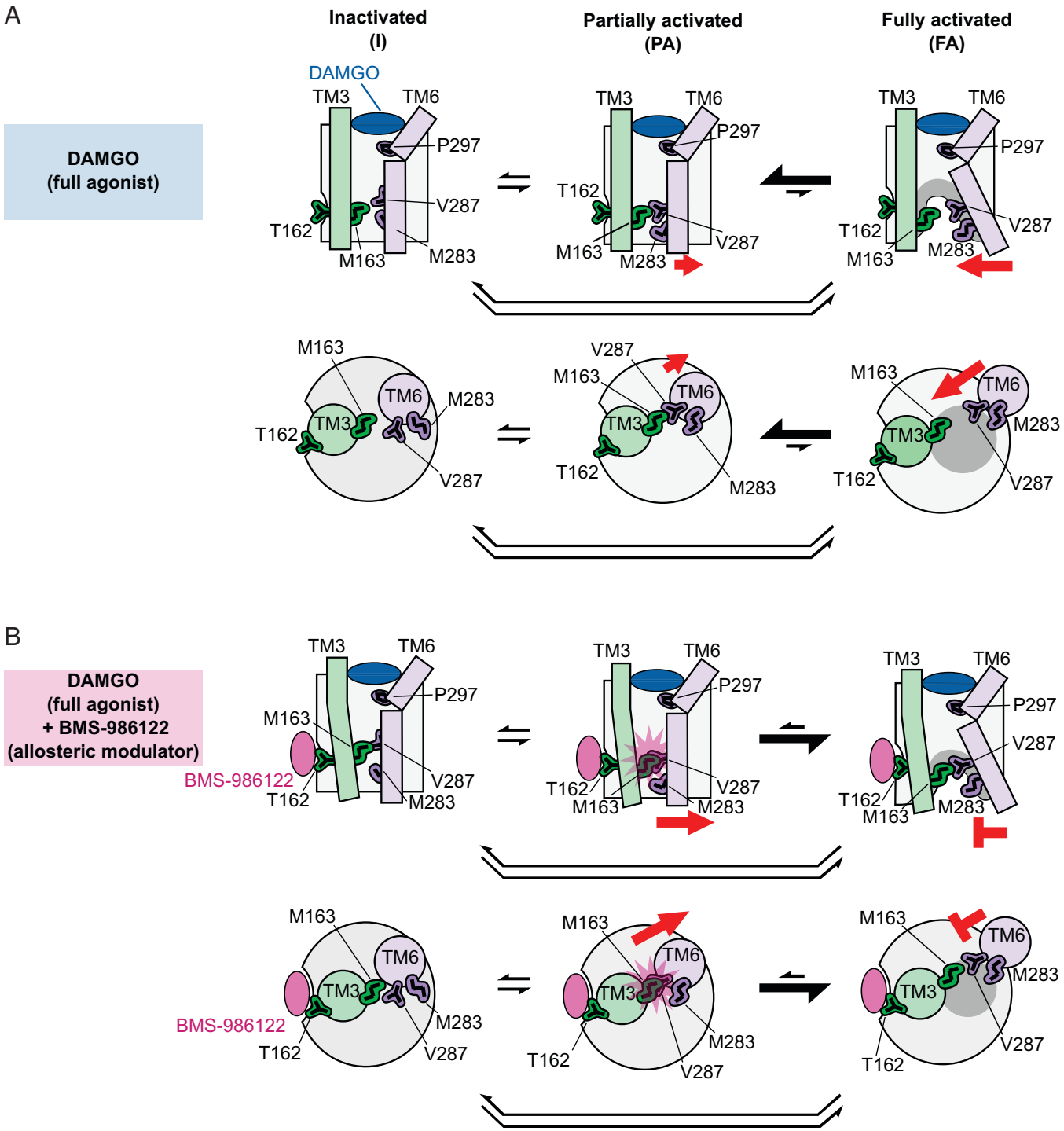

Fig. 5. Model of MOR activation regulated by the equilibrium shift caused by the allosteric modulator. Schematic diagrams of the conformational equilibrium at the intracellular half of TM6 in MOR. Models of function-related conformational equilibrium of MOR in the full agonist DAMGO-bound state (*A*) and the DAMGO-bound state in the presence of the allosteric modulator BMS-986122 (*B*). (*Upper*) Viewed parallel to the membrane. (*Lower*) Viewed from the intracellular side. MOR bound to the full agonist DAMGO exists in equilibrium between the inactivated, partially activated, and fully activated conformations. As compared with the inactivated conformation, the intracellular half of TM6 is rotated in the partially activated conformation and is rotated and outward-shifted in the fully activated conformation. Upon BMS-986122 binding to the region containing T162, the population of the fully activated conformation increases, because the steric clash between M163 and V287 stabilizes the intracellular half of TM6 in the outward-shifted position.

shed light on the development of novel analgesics targeting MOR, and other therapeutics for GPCR-related diseases.

Methods

The human MOR construct, MOR/Δ6M, and its variants were expressed in Sf9 (Invitrogen) or expreSF+ (Protein Sciences Corp.) cells and purified by cobalt affinity chromatography, FLAG affinity chromatography, and size-exclusion chromatography, as previously reported (6). Radioligand binding assays were performed by measuring competitive displacement of [^{3}H]diprenorphine (PerkinElmer) using increasing concentrations of DAMGO in the presence of vehicle (1% dimethyl sulfoxide [DMSO]) or BMS-986122. GTP turnover assays were performed by using a modified protocol of the GTPase-Glo assay (Promega) in the presence of vehicle (1% DMSO) or BMS-986122. All NMR measurements

were performed on Bruker Avance 600, 800, or 900 spectrometers equipped with cryogenic probes. Full experimental details can be found in *SI Appendix, SI Methods*.

Data Availability. All study data are included in the article and/or *SI Appendix*.

ACKNOWLEDGMENTS. This work was supported by grants from Japan Society for the Promotion of Science (JSPS) KAKENHI grant numbers JP17H06097 (to I.S.), JP21H02619 (to S.I.), JP20H03375 (to T.U.), JP19H04951 (to T.U.), JP21H02410 (to Y.K.), JP20K21473 (to Y.K.), and JP19H04946 (to Y.K.) and Japan Agency for Medical Research and Development (AMED) grant number JP18ae010104 (to I.S.).

1. D. M. Rosenbaum, S. G. F. Rasmussen, B. K. Kobilka, The structure and function of G-protein-coupled receptors. *Nature* **459**, 356–363 (2009).
2. R. Santos *et al.*, A comprehensive map of molecular drug targets. *Nat. Rev. Drug Discov.* **16**, 19–34 (2017).
3. B. K. Kobilka, X. Deupi, Conformational complexity of G-protein-coupled receptors. *Trends Pharmacol. Sci.* **28**, 397–406 (2007).
4. R. Schrage *et al.*, Agonists with supraphysiological efficacy at the muscarinic M_2 ACh receptor. *Br. J. Pharmacol.* **169**, 357–370 (2013).
5. R. Schrage, A. De Min, K. Hochheiser, E. Kostenis, K. Mohr, Superagonism at G protein-coupled receptors and beyond. *Br. J. Pharmacol.* **173**, 3018–3027 (2016).
6. J. Okude *et al.*, Identification of a conformational equilibrium that determines the efficacy and functional selectivity of the μ-opioid receptor. *Angew. Chem. Int. Ed. Engl.* **54**, 15771–15776 (2015).
7. X. Han, S. D. Tachado, H. Koziel, W. A. Boisvert, Leu128($^{3.43}$) (I128) and Val247($^{6.40}$) (V247) of CXCR1 are critical amino acid residues for g protein coupling and receptor activation. *PLoS One* **7**, e42765 (2012).
8. K. H. Ahn, C. E. Scott, R. Abrol, W. A. Goddard, 3rd, D. A. Kendall, Computationally-predicted CB1 cannabinoid receptor mutants show distinct patterns of salt-bridges that correlate with their level of constitutive activity reflected in G protein coupling levels, thermal stability, and ligand binding. *Proteins* **81**, 1304–1317 (2013).
9. P. J. Conn, A. Christopoulos, C. W. Lindsley, Allosteric modulators of GPCRs: A novel approach for the treatment of CNS disorders. *Nat. Rev. Drug Discov.* **8**, 41–54 (2009).
10. Y. Wang, Z. Yu, W. Xiao, S. Lu, J. Zhang, Allosteric binding sites at the receptor-lipid bilayer interface: Novel targets for GPCR drug discovery. *Drug Discov. Today* **26**, 690–703 (2021).
11. X. Liu *et al.*, An allosteric modulator binds to a conformational hub in the β_2 adrenergic receptor. *Nat. Chem. Biol.* **16**, 749–755 (2020).
12. N. Robertson *et al.*, Structure of the complement C5a receptor bound to the extra-helical antagonist NDT9513727. *Nature* **553**, 111–114 (2018).
13. J. Lu *et al.*, Structural basis for the cooperative allosteric activation of the free fatty acid receptor GPR40. *Nat. Struct. Mol. Biol.* **24**, 570–577 (2017).
14. A. C. Kruse *et al.*, Activation and allosteric modulation of a muscarinic acetylcholine receptor. *Nature* **504**, 101–106 (2013).
15. P. Xiao *et al.*, Ligand recognition and allosteric regulation of DRD1-Gs signaling complexes. *Cell* **184**, 943–956.e18 (2021).
16. J. Hughes, Biogenesis, release and inactivation of enkephalins and dynorphins. *Br. Med. Bull.* **39**, 17–24 (1983).
17. H. Akil, E. Young, J. M. Walker, S. J. Watson, The many possible roles of opioids and related peptides in stress-induced analgesia. *Ann. N. Y. Acad. Sci.* **467**, 140–153 (1986).
18. N. T. Burford *et al.*, Discovery of positive allosteric modulators and silent allosteric modulators of the μ-opioid receptor. *Proc. Natl. Acad. Sci. U.S.A.* **110**, 10830–10835 (2013).
19. P. Bisignano *et al.*, Ligand-based discovery of a new scaffold for allosteric modulation of the μ-opioid receptor. *J. Chem. Inf. Model.* **55**, 1836–1843 (2015).
20. D. Bartuzi, A. A. Kaczor, D. Matosiuk, Interplay between two allosteric sites and their influence on agonist binding in human μ opioid receptor. *J. Chem. Inf. Model.* **56**, 563–570 (2016).
21. N. T. Burford *et al.*, Discovery, synthesis, and molecular pharmacology of selective positive allosteric modulators of the δ-opioid receptor. *J. Med. Chem.* **58**, 4220–4229 (2015).
22. K. E. Livingston *et al.*, Pharmacologic evidence for a putative conserved allosteric site on opioid receptors. *Mol. Pharmacol.* **93**, 157–167 (2018).
23. R. Kandasamy *et al.*, Positive allosteric modulation of the mu-opioid receptor produces analgesia with reduced side effects. *Proc. Natl. Acad. Sci. U.S.A.* **118**, e2000017118 (2021).
24. N. T. Burford, J. R. Traynor, A. Alt, Positive allosteric modulators of the μ-opioid receptor: A novel approach for future pain medications. *Br. J. Pharmacol.* **172**, 277–286 (2015).
25. A. Manglik *et al.*, Crystal structure of the μ-opioid receptor bound to a morphinan antagonist. *Nature* **485**, 321–326 (2012).
26. W. Huang *et al.*, Structural insights into μ-opioid receptor activation. *Nature* **524**, 315–321 (2015).
27. A. Koehl *et al.*, Structure of the μ-opioid receptor-G_i protein complex. *Nature* **558**, 547–552 (2018).
28. S. G. Rasmussen *et al.*, Crystal structure of the β2 adrenergic receptor-Gs protein complex. *Nature* **477**, 549–555 (2011).
29. C. J. Draper-Joyce *et al.*, Structure of the adenosine-bound human adenosine A_1 receptor-G_i complex. *Nature* **558**, 559–563 (2018).
30. J. García-Nafría, R. Nehmé, P. C. Edwards, C. G. Tate, Cryo-EM structure of the serotonin 5-HT_{1B} receptor coupled to heterotrimeric G_o. *Nature* **558**, 620–623 (2018).
31. R. Sounier *et al.*, Propagation of conformational changes during μ-opioid receptor activation. *Nature* **524**, 375–378 (2015).
32. Y. Kofuku *et al.*, Efficacy of the β_2-adrenergic receptor is determined by conformational equilibrium in the transmembrane region. *Nat. Commun.* **3**, 1045 (2012).
33. J. Xu *et al.*, Conformational complexity and dynamics in a muscarinic receptor revealed by NMR spectroscopy. *Mol. Cell* **75**, 53–65.e7 (2019).
34. M. T. Eddy *et al.*, Allosteric coupling of drug binding and intracellular signaling in the A_{2A} adenosine receptor. *Cell* **172**, 68–80.e12 (2018).
35. S. Imai *et al.*, Structural equilibrium underlying ligand-dependent activation of β_2-adrenoreceptor. *Nat. Chem. Biol.* **16**, 430–439 (2020).
36. I. Shimada, T. Ueda, Y. Kofuku, M. T. Eddy, K. Wüthrich, GPCR drug discovery: Integrating solution NMR data with crystal and cryo-EM structures. *Nat. Rev. Drug Discov.* **18**, 59–82 (2019).
37. X. Cong *et al.*, Molecular insights into the biased signaling mechanism of the μ-opioid receptor. *Mol. Cell* **81**, 4165–4175.e6 (2021).
38. J. J. Liu, R. Horst, V. Katritch, R. C. Stevens, K. Wüthrich, Biased signaling pathways in β_2-adrenergic receptor characterized by ^{19}F-NMR. *Science* **335**, 1106–1110 (2012).
39. R. Nygaard *et al.*, The dynamic process of $\beta(_2)$-adrenergic receptor activation. *Cell* **152**, 532–542 (2013).
40. S. Isogai *et al.*, Backbone NMR reveals allosteric signal transduction networks in the β_1-adrenergic receptor. *Nature* **530**, 237–241 (2016).
41. I. Goba *et al.*, Probing the conformation states of neurotensin receptor 1 variants by NMR site-directed methyl labeling. *ChemBioChem* **22**, 139–146 (2021).
42. J. A. Ballesteros, H. Weinstein, Integrated methods for the construction of three-dimensional models and computational probing of structure-function relations in G protein-coupled receptors. *Methods. Neurosciences* **25**, 366–428 (1995).
43. Y. Kofuku *et al.*, Functional dynamics of deuterated β_2 -adrenergic receptor in lipid bilayers revealed by NMR spectroscopy. *Angew. Chem. Int. Ed. Engl.* **53**, 13376–13379 (2014).
44. H. Johansson *et al.*, Specific and nonspecific interactions in ultraweak protein-protein associations revealed by solvent paramagnetic relaxation enhancements. *J. Am. Chem. Soc.* **136**, 10277–10286 (2014).
45. T. Mizumura *et al.*, Activation of adenosine A_{2A} receptor by lipids from docosahexaenoic acid revealed by NMR. *Sci. Adv.* **6**, eaay8544 (2020).
46. S. Granier *et al.*, Structure of the δ-opioid receptor bound to naltrindole. *Nature* **485**, 400–404 (2012).
47. G. Fenalti *et al.*, Molecular control of δ-opioid receptor signalling. *Nature* **506**, 191–196 (2014).
48. T. Claff *et al.*, Elucidating the active δ-opioid receptor crystal structure with peptide and small-molecule agonists. *Sci. Adv.* **5**, eaax9115 (2019).
49. S. J. Perkins, K. Wüthrich, Ring current effects in the conformation dependent NMR chemical shifts of aliphatic protons in the basic pancreatic trypsin inhibitor. *Biochim. Biophys. Acta* **576**, 409–423 (1979).